

Steady-State Groundwater Flow Modeling of the MIU Site Area

Sean A. McKenna¹, Mehdi Eliassi¹, Kaoru Inaba², Hiromitsu Saegusa²

¹Sandia National Laboratories, Albuquerque, New Mexico, USA

²Japan Nuclear Cycle Development Institute



For submission to: Symposium on Groundwater Flow in Discrete Fractures, Japanese Geotechnical Society, Sept. 11-12, 2001, Tokyo

Abstract

Sandia National Laboratories (SNL) and Japan Nuclear Cycle Development Institute (JNC) constructed a steady-state flow model for the area surrounding the Mizunami Underground Laboratory (MIU) site in order to evaluate uncertainties due to hydrogeological model and groundwater flow simulation. A steady-state solution was determined for each of five different models. These five different models explore three different levels of complexity in the interpreted fault network at the MIU site, two different amounts of recharge and two different conceptualizations of hydraulic conductivity in the faults. A total of 24 particle tracks from specified starting locations were modeled. The location and velocities of particle tracks and the calculated F-ratio along each flowpath were calculated. One of the five models was then chosen for a more detailed level of calibration. The results of particle tracking both prior to and after calibration were then compared. The comparison of the heads predicted by each model to the observed heads in boreholes MIU-1, MIU-2, AN-1 and AN-3 shows variation in the quality of the predictions between the different models. The heads and the particle tracks are sensitive to the permeability of the fault network

Keywords: Evaluation of Uncertainty, Groundwater Flow at Depth, Geological Model, Discrete Feature, Groundwater Flow Analysis, Particle Tracking

Sandia is a multiprogram laboratory operated by Sandia Corporation, a Lockheed Martin Company, for the United States Department of Energy under contract DE-AC04-94-AL-85000

Introduction

The main objective of this work was to use the available data to construct a steady-state flow model for the area surrounding the MIU site. This report presents the work of one of six independent modeling groups working on the same problem. The work done by Sandia National Laboratories in cooperation with the Tono Geoscience Center consisted of a total of five different steady-state flow models. The five models were constructed to examine three different levels of complexity in the fault network, two different amounts of recharge to the granite and two different values of hydraulic conductivity in the fault network. Details of the five models are given below. The choice of the five models and the differences between them were left to each of the different modeling groups. One of the models was to then be chosen for a more detailed level of calibration (Model 6). For each of the six models, 24 particles are tracked from specified source locations to the model boundary. The results of particle tracking both prior to and after calibration are compared.

The groundwater flow and transport model, POR-SALSA, is used to construct the groundwater flow models shown in this report. POR-SALSA (Martinez, et al., 2001) is a three-dimensional finite element code, developed at Sandia National Laboratories for modeling groundwater flow and transport using massively parallel architecture. The results shown in this report were obtained by running POR-SALSA on the “Geo-Wolf” cluster of 36 PC’s linked together into a single super computer running the LINUX operating system. A total of 20 processors were used in these calculations, and the average run time to obtain a steady-state solution on the approximately 1 million-node model and track the 24 particles from the start locations to the model boundary was less than 6 minutes.

Model Domain and Boundary Conditions

The model domain chosen for this study is 4x5x3 kilometers (EW, NS, Vertical). The origin of the study area (lower southwest, or left hand, corner) has coordinates of: 3643.93, -71,044.5 and -3000.0 in the regional coordinate system used at the MIU site. An orthogonal, mesh with uniform node spacing of 40 meters in each direction is used to define a grid that is 101 (nx) by 126 (ny) by 76 (nz) nodes (total of 967,176 nodes). This domain is roughly centered on the MIU site and the southern boundary approximates the location of the Toki River.

The top of the domain is set to an elevation of 0.0 meters. The sedimentary units are not included in the model domain as they are generally above this elevation. Borehole data analyzed by Rautman and McKenna (in review) indicate that the upper, relatively high fracture frequency zone in the granite occurs between an elevation of 0.0 and -120.0 meters. While there is variation in the elevation and thickness of this upper high fracture frequency zone, for the modeling work reported here, this zone is assumed to be uniformly 120 meters thick. Regions below this elevation are composed of a lower fracture frequency region and the Tsukyoshi Fault.

A recharge rate of 7.49E-09 m/sec (233mm/year) was determined as an average recharge value from data provided by JNC. This recharge rate is assigned as a flux boundary across the top of the model domain. It is noted that this recharge rate is measured at the land surface and is a measurement of the amount of recharge entering the sedimentary units overlying the granite. For this work, it is assumed that all of the recharge entering the sedimentary units also enters the granite.

The sides and bottom of the model are assigned as no-flow boundaries. Boundary head values were obtained from JNC from a regional modeling study to apply as side and end boundary conditions; however, these head values did not account for faults that were included in the present modeling. The end boundaries are set to the initial head values and are then fixed throughout the simulation. The initial head values are determined as the ground surface elevation minus 120 meters. The value of 120 meters was determined through a brief trial and error calibration process.

Model Definition and Properties

The five different models considered in this study are defined in Table 1. The main focus of this study was consideration of the changes in calibration and particle tracking results that occur as the number of faults and the fault properties are changed. The surface traces of the different faults are the result of an extensive lineament analysis (Maeda, pers. comm.). Models 1, 2 and 3 examine different fault networks, all as low K barriers to flow. Model 4 examines a decrease in the amount of recharge entering the top of the model using the same fault network as Model 2. Model 5 also uses the same fault network as Model 2, but considers all faults, other than the Tsukyoshi Fault, to be high K units. Model 6 is the better calibrated version of model 2 with an upgradient boundary face that fixes the heads as increasing by 1 meter for each 40 meters of depth below the top of the model. Figure 1 shows the 3 different fault networks used in this study along with an example image of the assigned K values used in the study.

Table 1. Definition of the models examined in this study.

Model Number	Model Description
1	1 Fault
2	7 Faults (longest lineaments and faults confirmed in DH-4 and DH-2)
3	33 Faults (all lineaments on lineament map from JNC)
4	Same as Model 2 with 10 percent less recharge
5	Same as Model 2 with faults other than Tsukyoshi assigned as high K
6	Same as Model 2 with different fixed heads on upstream boundary

The hydraulic conductivity and porosity values assigned to the different units within the model are given in Table 2. The K values for the Upper and Lower Fractured Domains are taken as rough averages of the hydraulic testing done over 100 meter long intervals by JNC. The K values for the faults are assumed values, as are all porosity values. It is

noted that the properties of the Tsukyoshi Fault are held constant across all 6 Models. The values of the other faults are changed to the High K Fault value for Model 5.

Table 2. Model properties.

Material	Hydraulic Conductivity (m/s)	Porosity	Comments
Low K Faults	5.0E-09	0.005	Tsukyoshi Fault is fixed at this value in all models. All other faults use this value except for model 5.
Upper Fractured Domain	5.0E-06	0.10	Used in all models
Lower Fractured Domain	5.0E-08	0.01	Used in all models, largest fraction of model domain
High K Faults (Conduits)	5.0E-06	0.05	Only used in Model 5

Model Results

The model results are presented in terms of the calculated steady-state head field, the calibration of the modeled heads as compared to observed heads in boreholes MIU-1, MIU-2, AN-1 and AN-3 and the particle tracking results.

Calculated Heads

The head fields for each of the 6 different models are shown in Figure 2. The number of low permeability faults included in the model increases from Model 1 (1 fault) through Model 3 (33 faults). The inclusion of additional faults in the model tends to create higher heads in the north end of the fault. The fixed head boundary on the upstream face of the model does not change, but steep local gradients develop where the groundwater flow is suppressed by the lower permeability faults. Also, the recharge applied to the top boundary cannot dissipate as rapidly from regions of the model that are surrounded by low permeability faults. As an example of this result, the head distribution for Model 3 shows an obviously fault bounded region of high head along the western model boundary in the northern half of the domain (see Figure 2, center left image).

The model result with the lowest average head values is Model 5. The inclusion of six long faults as high K conduits allows the head to easily dissipate as flow is channeled through these conduits from the northern to southern portions of the model.

Calibration

The first 5 models were not calibrated in any way. The steady-state head values are simply those that result from the choice of boundary conditions and material properties. The comparison of these simulated heads to the measured heads in the MIU-1, MIU-2, AN-1 and AN-3 boreholes is shown in Figure 3.

Examination of the graphs in Figure 3 shows that no single model does the best job of reproducing the observed heads across all piezometer locations. However, several of the models produce consistently poor matches to the observed head. For example, Model 5 always underpredicts the observed head values. In general, Model 5 underpredicts the heads by approximately 20 meters with the exception of at the MIU-2 borehole where Model 5 underpredicts the observed heads by approximately 50 meters. The reason for the consistent underprediction of heads by Model 5 is interpreted to be the inclusion of the faults as high K pathways for flow. The head in the region cannot build up to the proper levels as it is dissipated through the high K pathways.

Contrary to the underprediction of heads by Model 5, Model 3 consistently overpredicts the observed heads. With the exception of the lower piezometer locations in MIU-2, which are slightly underpredicted, Model 3 overpredicts the measured heads by 10-50 meters (Figure 3). Model 3 contains all 33 faults and they are all set to the same relatively low K value. The presence of these low K barriers to flow causes the flow to be impeded and the modeled heads to be higher than the observed heads.

Models 1 and 2 produce heads that are generally in the same range as the observed heads, with the exception of the piezometers below the fault in MIU-2. Figure 3 shows that the predicted heads are closest to the observed heads in boreholes AN-1 and AN-3. Compared to the observed heads in MIU-2, Models 1 and 2 slightly overpredict the top most piezometer significantly underpredict the heads measured at the lower piezometers (those below the Tsukyoshi Fault).

The heads predicted by Model 4 show the same pattern as those predicted by Model 2, but with absolute values of the predicted heads that are approximately 8 to 10 meters lower than those predicted by Model 2. This decrease in the predicted heads is solely due to the 10 percent decrease in the amount of recharge applied to the top of Model 4 relative to Model 2. The assumption made in this modeling study is that all of the recharge to the overlying sedimentary units is transmitted directly to the granitic rocks. This may be an overestimation of the amount of recharge. Figure 3 shows that at boreholes MIU-1 and AN-1, the modeled heads tend to show a larger vertical gradient (higher heads at higher elevations) than do the observed heads. These results suggest that the amount of recharge entering the granite may be overestimated in the models. It is interesting to note that the lack of a vertical gradient in the AN-3 observations is well matched by the models. The AN-3 observations are only available at the top of the borehole in the upper highly fractured domain. The correct prediction of no vertical gradient in this layer indicates that the K value assigned to this layer in the models is high enough to not create a significant head loss across this layer and this reproduces the observed behavior of the groundwater system.

Model 6 is the single attempt at a better calibration of the model to the observed heads. This calibration was done by increasing the heads at the northern end of the domain as a function of depth. An additional 1-meter of head for every 40 meter decrease in elevation is added to the fixed head boundary condition on the north end of the model. The fault geometry and the material properties for Model 6 are the same as those used in Model 2.

One major observation from the comparison of the observed heads to the modeled heads for Models 1 through 5 is that the observed heads below the Tsukyoshi Fault in MIU-2 are considerably higher than those predicted by the models. This discrepancy could be caused by higher heads at depth due to recharge at higher elevations to the north of the model domain. In order to simulate this conceptual model, the heads at the north end of the domain are increased with depth. This change creates the predicted heads shown in Figure 2 for Model 6.

The results of Model 6 are similar to those of Model 3 in that the observed heads are generally overpredicted. Model 6 does produce nearly accurate head values below the Tsukyoshi Fault in MIU-2, but this is the only set of piezometer locations that are accurately modeled.

Particle Tracking

Particle tracking is accomplished using each of the steady-state head fields created for the 6 different models. The particle tracking code, TRACKWAY, developed at Sandia National Laboratories is used to determine the pathways. TRACKWAY uses the potential field of the steady-state head field to determine the X,Y and Z coordinates of a groundwater streamline at any time after the particle start. The theory employed in TRACKWAY is based on that developed by Pollock (1989) for the USGS MODPATH program.

The starting locations for the 24 particles, determined by JNC to assess travel times from different locations to the model boundary, are arranged in 6 different vertical columns. The X and Y coordinates of the columns are given in Table 3. At each column, four particles are released at elevations of -250, -500, -750 and -1000 meters.

Table 3. The starting coordinates of the particles.

Particle Numbers and Elevation	X coordinate	Y coordinate
1(-250) 4(-500) 7(-750) 10 (-1000)	4489.0	-66,900.0
2(-250) 5(-500) 8(-750) 11 (-1000)	5489.0	-66,900.0
3(-250) 6(-500) 9(-750) 12 (-1000)	6489.0	-66,900.0
13(-250) 16(-500) 19(-750) 22 (-1000)	4489.0	-68,630.0
14(-250) 17(-500) 20(-750) 23 (-1000)	5489.0	-68,630.0
15(-250) 18(-500) 21(-750) 24 (-1000)	6489.0	-68,630.0

Three-dimensional images of the particle tracking results are shown in Figure 4. The gray-scale in Figure 4 shows the instantaneous particle velocity in meters per year. One unexpected result of the particle tracking is that, in Model 1, the particles with the easternmost starting location to the north of the Tsukyoshi Fault leave the model at the upstream boundary. This result is caused by the low head value on the eastern side of the northern boundary where the Hiyoshi River valley exits the model domain. This result is consistent with the Hiyoshi River acting as a discharge zone.

This same condition of particles exiting the northern boundary of the domain also exists for all of the other models. Depending on the fault geometry used in the model and the

properties assigned to the faults, other particles from the center column of starting locations to the north of the Tsukyoshi Fault will also exit the model at the northern boundary. Model 5, with the high hydraulic conductivity faults, causes 7 of the 24 particles to exit the northern boundary of the model. The decrease in the recharge value as calculated in Model 4 does not affect the number of particles exiting at the northern boundary relative to Model 2.

The largest change in the positions of the streamlines is caused by the conceptualization of the faults as high hydraulic conductivity pathways in Model 5. The NE-trending fault in the northeast portion of the model domain causes 7 of the particles to exit the domain along the northern boundary. In the SE portion of the model domain, two faults are included with steep dips to the south (see upper right image in Figure 1). The northernmost of these two faults has a dip angle determined from interception of the fault in the DH-2 borehole. The southernmost of these two faults is assigned a dip equal to that of the Tsukyoshi Fault based on the similarity of the strike of this fault and that of the Tsukyoshi fault. These two faults control the paths of the particles starting on the easternmost column south of the Tsukyoshi Fault. The two faults together provide a high K pathway from the surface of the model (relatively high head) to the southern boundary (relatively low head). Once the particles enter this high K pathway, the hydraulic conductivity contrast between the high K fault and the lower K background rock keeps the particles in the fault zone until they reach the no-flow boundary at the bottom of the model. After reaching the bottom of the model, they then migrate to the southern, constant head, boundary and exit the domain.

In addition to creating significant differences in the paths of the particles, the high K faults in Model 5 also cause a significant change in the velocity of the particles. Inside the high K faults, the velocities are generally greater than 20m/year and can reach velocities in excess of 500 meters per year. This increase in velocity is shown by the large amount of light color along the streamlines in the lower left image of Figure 4.

Distributions of travel times, travel lengths and the F-ratio are given in Figure 5 as box and whisker plots. The travel times and path lengths are calculated directly from the particle tracking results.

The F-ratio can be thought of conceptually as a ratio of the factors resisting transport: the path distance and the surface area available for diffusion to the factors driving transport—the advective velocity. The F-ratio is defined as (After SKI, 1997):

$$F = \frac{(Distance)(Surface)}{V_{Darcy}} = \frac{(Time)(Surface)}{Porosity}$$

The F-ratio calculations require several assumptions on the average fracture frequency and the amount of the fracture surface that is actually in contact with zones of significant advection in the fracture itself. The specific surface is defined as the fracture surface area in contact with the transport pathway per volume of rock. For these calculations, the average fracture frequency is assumed to be two fractures per meter. This frequency is

assumed to be isotropic and is in line with fracture frequencies observed in the analysis done by Rautman and McKenna (in review). This fracture frequency results in 6 fractures per cubic meter of rock (2 fractures in each of 3 orthogonal fracture sets). Each fracture is assumed to be composed of two parallel plates separated by the fracture aperture. Counting each plate (face) of the fracture as a surface, the total fracture surface per cubic meter of rock is 12 m^2 . For the calculation of the F-ratio, the proportion of the fracture surface in contact with actively flowing water is assumed to be 5 percent. These assumptions result in a specific surface of 0.6 m^{-1} . It is noted that the values of the F-ratio are fully dependent on the assumptions made regarding fracture frequency and the percent of the surface area in contact with the flowing water. At this time, it is not possible to make in-situ measurements of the second of these two parameters.

The travel time of each particle and the arithmetic average of the porosity along each pathway are used with the assumed value of the specific surface to calculate the F-ratio. The distributions of the calculated F-ratios for each model are shown in the bottom image of Figure 5. Although not shown in this report, the average porosity along the flow paths is close to porosity assigned to the low fracture zone for models with the exception of Model 5 where it is significantly higher. This increase in the fracture porosity and the shorter travel times decreases the F-ratios for Model 5 relative to the other models (bottom image, Figure 5).

Summary

A total of 5 models were created to examine the effects of fault networks, recharge and the hydraulic properties of faults on the location and velocities of particle tracks and the calculated F-ratio along each flowpath. The comparison of the heads predicted by each model to the observed heads in boreholes MIU-1, MIU-2, AN-1 and AN-3 shows variation in the quality of the predictions between the different models.

The model with the largest number of low conductivity faults (Model 3) overpredicts the measured heads and the model with the high conductivity faults (Model 5) underpredicts the measured heads. A sixth model with a modified fixed head boundary on the northern boundary was created to better match the observed heads in MIU-2 below the Tsukyoshi Fault. This sixth model does better match the observed heads in the lower portions of MIU-2; however, this model does not accurately predict the other head observations.

The particle tracking results show that the distribution of travel times, travel lengths and F-ratios are similar across 6 models with the exception of the Model 5 results. The high conductivity pathways in Model 5 cause shorter travel times and correspondingly smaller F-ratio values. However, this model does not reproduce the observed heads and may be a poor conceptualization.

This modeling exercise has brought to focus a number of issues that will be considered in future work. First of all, the hydraulic conductivity value assigned to the Tsukyoshi Fault in this work may be too high. Additional calibration studies where the K value assigned to the Tsukyoshi Fault is varied will be conducted. Also, new information from the drilling and monitoring of DH-12 indicates that the Toki river at the south end of the

model domain is a regional discharge boundary. This boundary condition will be incorporated in the next version of the model. Finally, there is also new information from the drilling and hydrotesting of the MIU-4 and DH-13 boreholes that will be incorporated into the next generation model.

References:

- McKenna, S.A. and C.A. Rautman, (in review), Stochastic Modeling of Fracture Frequency along a Cross-Section at the MIU Site, Tono Region, Japan, Sandia National Laboratories, Albuquerque, New Mexico, 122 pp.
- Martinez, M.J., P.L. Hopkins, P.C. Reeves, 2001, PorSalsa User's Manual, SAND95-2752, Sandia National Laboratories, Albuquerque, New Mexico.
- Pollock, D.W., 1989, Documentation of computer programs to compute and display pathlines using results from the U.S. Geological Survey modular, three-dimensional finite-difference ground-water flow model: U.S. Geological Survey, OFR 89-381, 188 pp.
- SKI, 1997, SKI Site-94 Deep repository performance assessment project, Swedish Nuclear Power Inspectorate, SKI Report 97:5, Stockholm, Sweden.

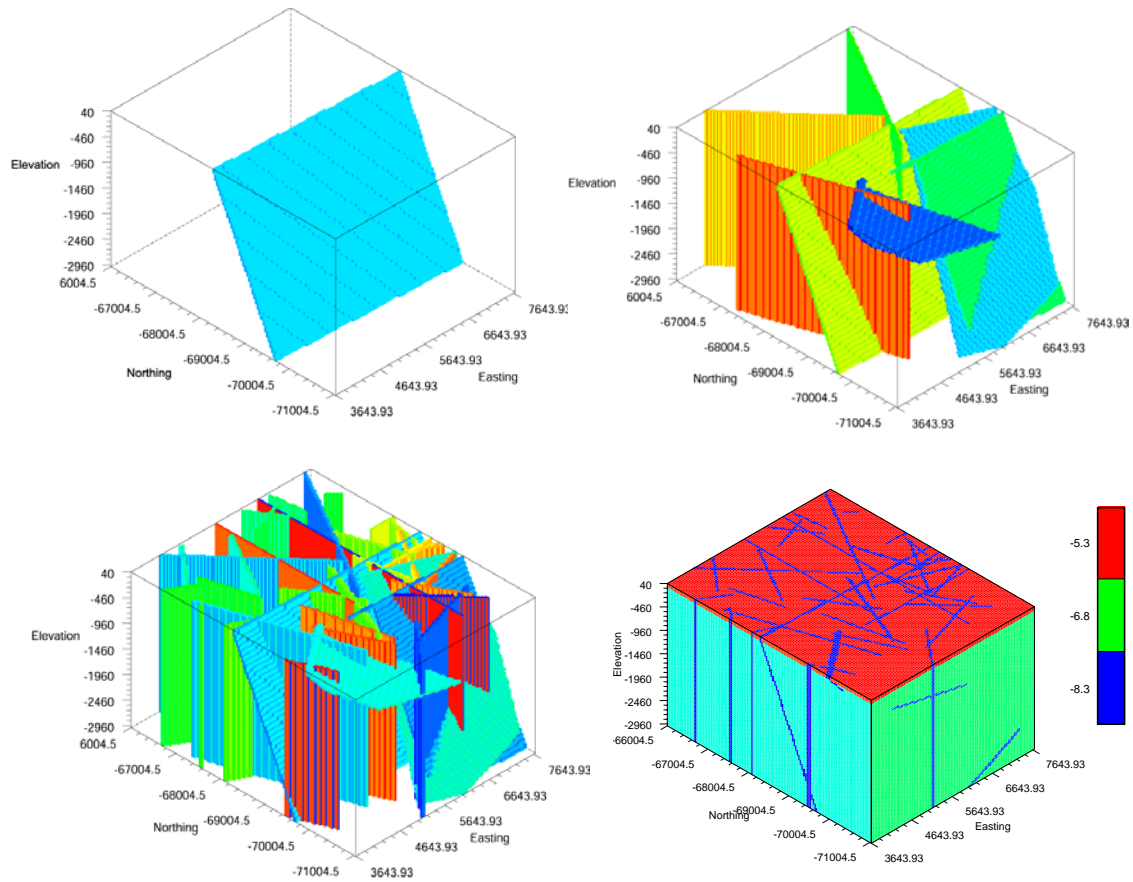


Figure 1. Images of the three fault networks used in the models (upper images and lower left image) and an example (Model 3) of the hydraulic conductivity values assigned to the model domain. The fault networks are used in Model 1 (upper left), Models 2, 4, 5 and 6 (upper right) and Model 3 (lower left).

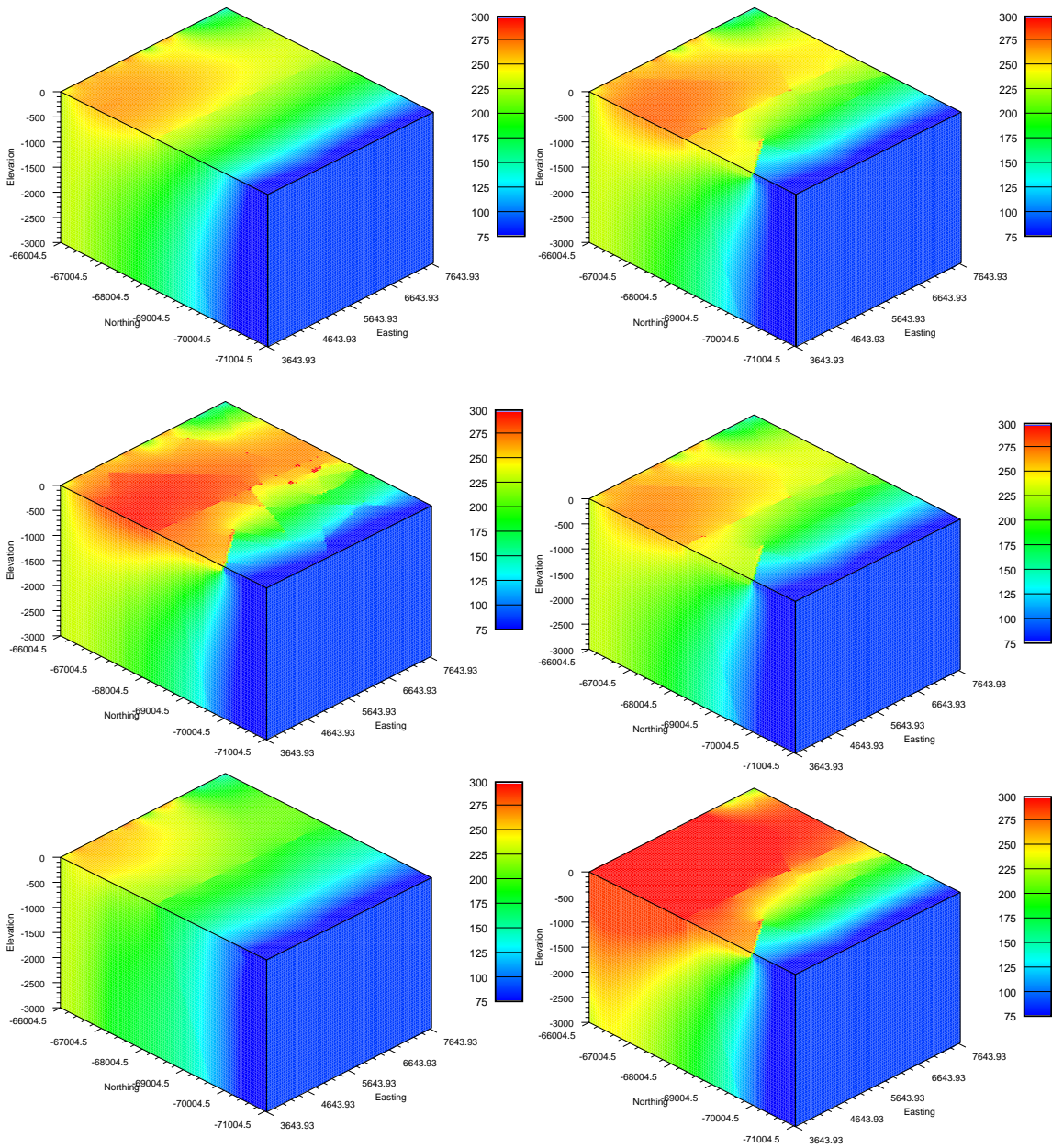


Figure 2. Calculated steady-state head fields for Models 1 (upper left), 2 (upper right), 3 (center left), 4 (center right), 5 (lower left) and 6 (lower right). The color scale shows head in meters above sea level. North is to the upper left in each image.

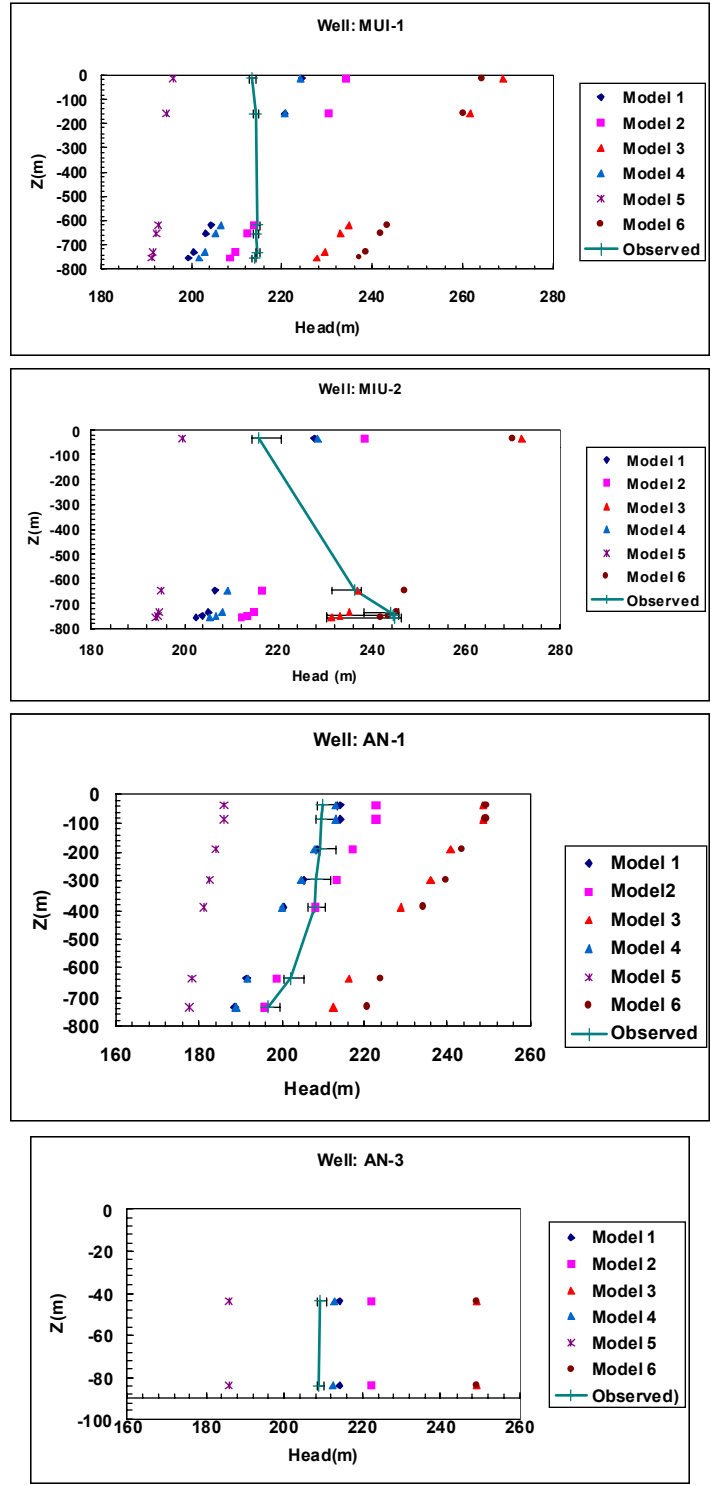


Figure 3. Comparison of modeled heads and measured heads at the MIU-1, MIU-2, AN-1 and AN-3 boreholes.

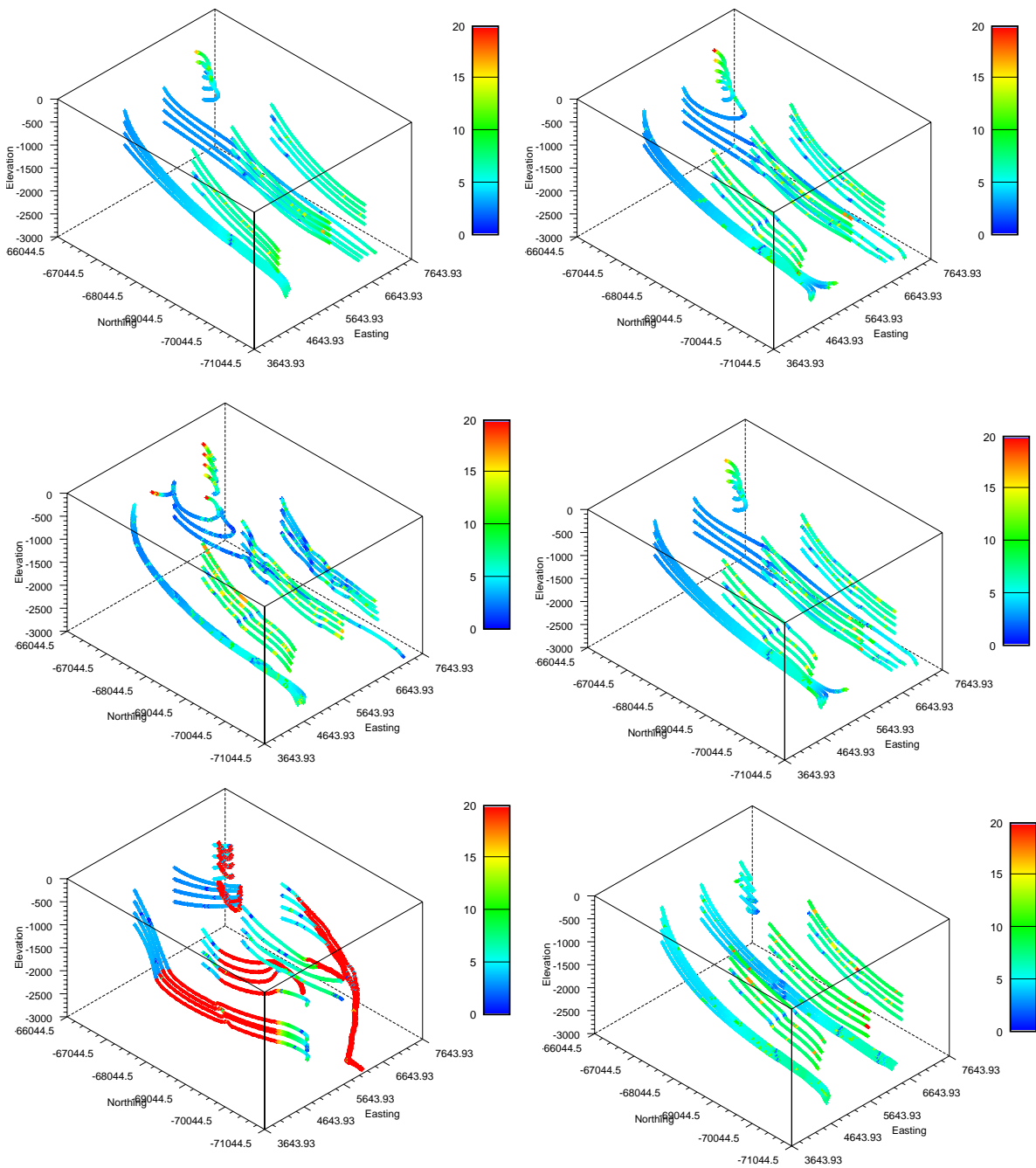


Figure 4. Three-dimensional views of the particle track locations for Models 1 (upper left), 2 (upper right), 3 (center left), 4 (center right), 5 (lower left) and 6 (lower right). The color scale shows instantaneous particle velocity in meters per year.

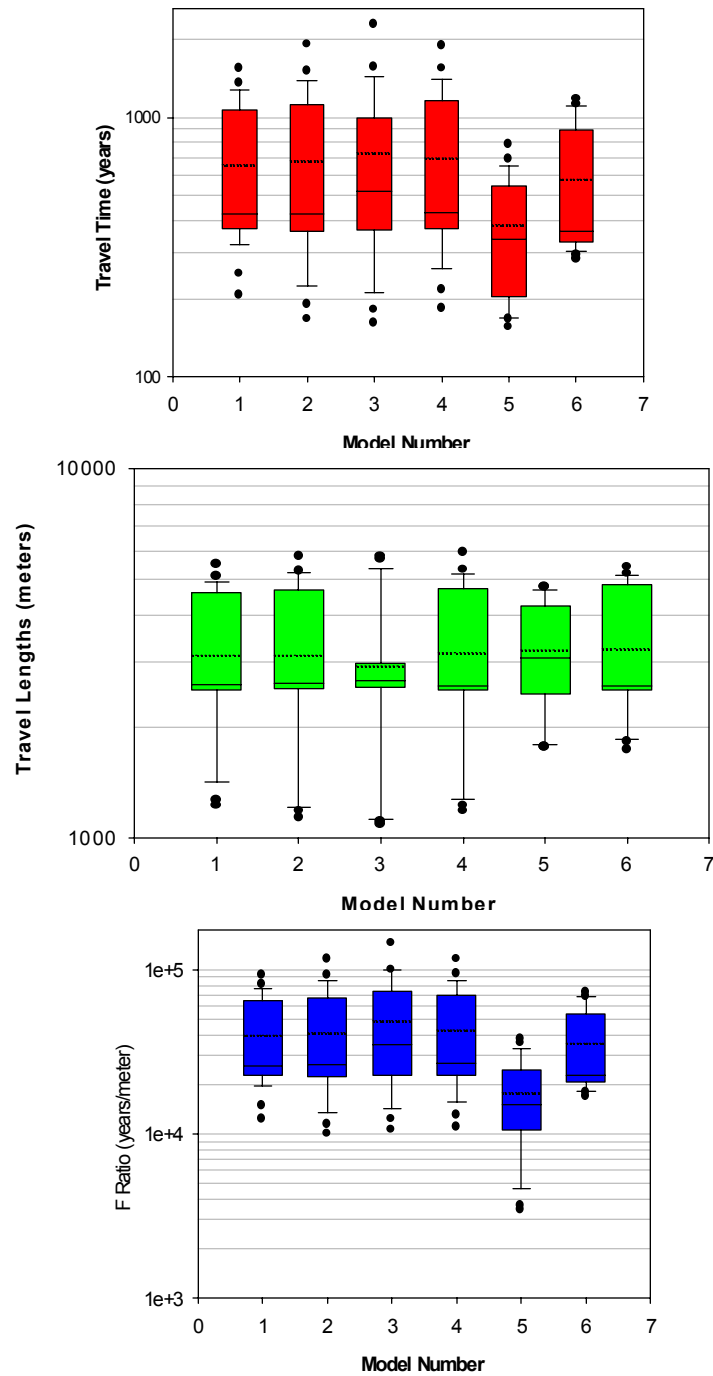


Figure 5. Distributions of travel times (top image), travel lengths (middle image) and F-ratio (bottom image) for the 6 models. Each distribution is defined by 24 streamlines. The dashed line indicates the mean and the solid line indicates the median. The top and bottom of the colored boxes are the 75th and 25th percentile values respectively. The whiskers extend to the 5th and 95th percentile values. Values beyond the 5th or 95th percentile lines are shown as circles.